INTELLIGENT LOADING TESTS ON STEEL BEAM-COLUMNS UNDER VARYING AXIAL AND LATERAL LOADS

by

Ken-ichi OHI(I), Koichi TAKANASHI(II), Yiyi CHEN(III), and Hideo KONDO(IV)

1. INTRODUCTION

When a high-rise or middle-rise building is subjected to horizontal earthquake loads, its side columns are subjected to not only varying lateral loads but also varying axial loads due to overturning. A lot of experimental studies were made on inelastic behaviors of steel beam-columns under constant axial loads[1][2], but few were made on those under varying axial loads.

In the fields of reinforced concrete structure, several experimental studies in consideration of varying axial loads were reported[3][4][5]. In these studies, the change of axial load is usually controlled to be proportional to the magnitude of lateral load until it reaches to a certain specified load value, and after that, the axial load is kept constant. Such a loading program given a priori may be justified for the case that the over all load carrying capacity of the frame is not so much influenced by the resistance of the column to be tested, for example, in the case of weak-beam type frame. In the case of weak-column type frame, however, the load carrying capacity of the frame and then the magnitude of overturning are strongly controlled by the resistance of the column to be tested. In such a case, the axial load change is desired to be determined dynamically from the resistance of the column measured during the loading test.

In this paper, an intelligent loading program about axial load change is made possible by use of sub-structuring techniques in a computer-controlled testing system. Loading tests are performed on H-shaped steel beam-columns, which are assumed to be side columns at the lowest story of a tower-like building. Also, analyses based on a simple inelastic beam-column model proposed by the authors[6] are carried out in order to check its applicability to the beam-columns under varying axial loads.

2. INTELLIGENT LOADING TEST

Consider a fictitious structural system as shown in Fig. 1. A rigid body is supported by a single column and an idealistic pin-roller support. A lateral load and a vertical load, denoted by F and $2N_c$ respectively, are applied to the geometrical center of the rigid body. The column foot is pinned to the basement and the column top is connected rigidly to the rigid body. The vertical displacement at the pin-roller support is constrained to be the same with the vertical displacement at the column top, that is, it is assumed that the rigid body does not rotate. In the following loading tests, the column in the fictitious structural system is tested as a cantilever beam-column subject to varying axial and lateral loads. From the equilibrium condition on the rigid body shown in Fig. 2, the axial load change, denoted by N_{ov}, is derived as:

$$N_{ov} = (KLF + M)/H \qquad (1)$$

where KL: Height of loading point from the column top
H: Distance between the column top and the pin-roller support
L: Column length
F: Lateral resistance, M: Bending moment at the column top

(I) Associate Professor, Institute of Industrial Science, University of Tokyo,
(II) Professor, dittos, (III) Research Associate, dittos, (IV) Technical Associate, dittos.

In the following tests, the resistance terms in Eq. (1), F and M, are measured from the loading test and used to determine the axial load change to be applied to the specimen. The values of KL and H are set to 10L and L, respectively. The test setup used is shown in Fig. 3, where the column specimen is connected to the rigid loading beam and loaded by two jacks at the central joint and the pin–roller support. Main data measured during the tests are (1) the load applied by the transverse actuator at the central joint, P, (2) the load applied by the other jack in the axial direction, N^*, (3) the transverse displacement at the central joint, δ_o, and (4) the rotation at the central joint, θ. The bending moment at the central joint is calculated by:

$$M = N^* \delta_o + F^* L_1 \tag{2}$$

where F^* is the reaction force at the support and evaluated by:

$$F^* = L_2 P / (L_1 + L_2) \tag{3}$$

The column axial force denoted by N ($= N_c + N_{ov}$), the lateral resistance denoted by F, and the lateral displacement denoted by δ, in the fictitious structural system shall satisfy the following geometrical relations:

$$N = N^* \cos\theta + F^* \sin\theta \tag{4}$$
$$F = F^* \cos\theta - N^* \sin\theta \tag{5}$$
$$\delta = \delta_o \cos\theta + L_1 \sin\theta \tag{6}$$

Displacement control for the transverse actuator and load control for the axial actuator are adopted during the test procedure. Every time after the transverse actuator is driven in a bit by bit manner, P, N^*, δ_o, and θ are measured and used to determine the new axial load so that Eqs. (1) to (5) shall be satisfied. And then the command signal corresponding to the new axial load is transmitted to the controller of the axial jack. So far as the loading is made in a quasi–static manner, such a test control may be performed slowly and easily supervised even by a small microcomputer.

Test specimens are hot–rolled H–shaped members, and their nominal cross–sectional sizes are commonly H–150x150x7x10. The measured dimensions of the specimens and the loading conditions are summarized in Table 1. Monotonic loading tests and cyclic loading test were performed. Two kinds of monotonic loading were considered: one case is that the compression force in the column increases according as the magnitude of the lateral load increases. We call this loading case simply as 'compression side' loading hereafter. The other case is that the compression force decreases according as the magnitude of the lateral load increases. Similarly, this loading case is referred as 'tension side' loading hereafter. Initial axial load, N_c, is commonly set to 53.6 tons, 40 percent of the yield axial load. Cyclic loading tests were performed according to the loading program shown in Fig. 5. The cases of the constant axial loads are also tested for the comparison. The constant axial loads in the monotonic loading are set to the peak axial loads (the minimum or the maximum) observed in the cases of varying axial loads. The constant axial loads in the cyclic loading is identical to the initial axial load. The results of the tension tests on the test pieces taken from the flange and the web are summarized in Table 2, and the compression tests on stub–column specimens are summarized in Table 3.

3. TEST RESULTS

The lateral resistance vs. displacement curves observed in the monotonic loading tests are shown in Figs. 6(a) and 7(a). The lateral resistance vs. displacement curves observed in the cyclic loading tests are shown in Figs. 9(a) and 10(a). Also, the end moment vs. axial load trajectories are shown in Figs. 8(a) and 8(b). For every specimen, the local buckling failure is commonly detected at the column end during the loading tests. It should be noted, however, that

the deterioration of the lateral resistance are mostly caused by so-called P-Δ effect or the secondary moment due to the high axial load and the large displacement. The followings are read from these figures:

The maximum lateral resistance observed in the 'compression side' loading is almost the same with the maximum resistance detected in the corresponding case of constant axial load. On the contrary, the maximum lateral resistance in the 'tension side' loading is about 15 % lower than the resistance observed in the corresponding case of constant axial load. Possible explanation about this difference is: the maximum lateral resistance in the 'compression side' loading is limited by the P-Δ effect due to relatively high axial load. On the other hand, the maximum lateral resistance in the 'tension side' loading is rather limited by the local buckling failure, which seems to be initiated and brought up gradually before the maximum resistance is detected. In the initial stage of the yielding in the 'tension side' loading, the column is subjected to higher axial load and then more prone to the local buckling than the column under the corresponding constant axial load.

The manners of the lateral resistance deterioration observed under the varying axial loads are considerably different from those observed in the corresponding constant axial load cases, and also they depend on whether the loading case is 'tension side' or 'compression side.' While the deterioration observed in the 'compression side' is less severe than that in the case of the constant axial load, the lateral resistance in 'the tension side' compression drops abruptly and severely.

Such a difference can be explained as follows: In the 'compression side' loading, (i) the deterioration of the lateral resistance leads to, (ii) the decrease of the overturning in the structure as well as the compression force in the column, and then (iii) the P-Δ effect diminishes. Such a converging cycle will act as a sort of moderator against the resistance deterioration. On the contrary in the 'tension side' loading, (i) the deterioration of the lateral resistance leads to, (ii) the decrease of the overturning in the structure but the increase of the compression force in the column, and then results in (iii) the increase of the P-Δ effect. Such an accelerating process will induce a sudden drop of the lateral resistance and very brittle behaviors.

From the behaviors of the stress point, (M, N), shown in Fig. 8, one can imagine the existence of the limiting surface or the yield surface in (M, N) space, and the dashed lines shown in Fig. 8 are the approximated interaction formula between the fully plastic moment (bent about strong axis of H-shaped cross-section) and the axial force. Since the dashed lines are drawn on the basis of the initial yield stress, the actual stress point goes outside of these limits, that is, the actual yield surface is inflated due to strain-hardening. It is also seen that the actual yield surface is diminishing after some inflation, and this must be related to the local buckling failure.

4. ANALYSIS

(1) Simple Beam-column Model[6]

A steel beam-column cantilever is regarded herein as an assembly of two elements as shown in Fig. 11: one is an elastic beam, and the other is an inelastic joint. In the following analysis, nodes are located at the tips of these two elements. Geometrical non-linearity or P-Δ effect is considered only for the nodal displacements by updating each element coordinate system in the incremental analysis.

The inelastic joint consists of four axial springs and a shear panel as shown in Fig. 12. In the presence of the stress transmission among the springs and the panel, each spring may carry axial force varying along the joint length, but the axial force at the center is chosen as the representative axial force of each spring.

Two different skeleton curves are used for the tension-side and the compression-side behaviors of each spring, respectively. The tension-side skeleton curve shall be arranged similar to the uni-axial stress-strain curve of steel material, and the compression side skeleton curve shall be arranged in consideration of the strength deterioration due to local buckling. Piecewise linear models are adopted herein for the both side skeletons as shown in Fig. 13(a).

Two imaginary points termed 'target points' on the skeleton curves, one for each side, are considered herein. These points are referred to determine unloading and reloading paths. Each target point is set to the elastic-limit point as the initial state. When a loading beyond the elastic-limit is made along one side skeleton with a certain amount of plastic displacement increment, the target point of the loading side moves together with the loading point, and at the same time, the other side skeleton curve including the other target point shall be shifted to the loading direction as much as Ψ times the displacement increment. Such a loading procedure on the skeleton curve is illustrated in Fig. 13(b). If Ψ is set to zero, neither hardening nor degrading occurs during cyclic reversals within the past peak amplitudes. If Ψ is set to one, the hysteresis includes no softening due to the Bauschinger's effect. Actual behaviors of steel members are believed to fall on the intermediate states between these two extremes.

Unloading and reloading paths are modeled as portions of the Ramberg-Osgood function, denoted by $\delta = R_{-O}(P)$. The parameters included in this function is determined to satisfy (i) $\delta_U = R_{-O}(P_U)$, where the point (δ_U, P_U) is the last unloading point, (ii) $\delta_T = R_{-O}(P_T)$, where the point (δ_T, P_T) is the target point on the skeleton curve in the unloading and reloading direction, and (iii) $K_1 \, d R_{-O} / dP (P_U)=1$ where K_1 is the initial elastic stiffness. These conditions are illustrated in Fig. 13(c). The tangent stiffness denoted by $K^*(=dP/d\delta)$ is derived from these conditions as:

$$K^* = K_1 K_a / [K_a + (K_1-K_a)|(P-P_U)/(P_T-P_U)|^{r-1}] \quad (7)$$

$$\text{where } K_a = (P_T-P_U)/(\delta_T-\delta_U) \quad (8)$$

(2) Results of the Analysis

The yield stress and the maximum tensile strength needed to arrange the tension-side skeleton curve can be derived from the tension test results summarized in Table 1. As for the compression-side skeleton curve, it is empirically recognized that the maximum moment capacity of the beam-column would be underestimated if the maximum stress(σ_m) derived from the stub column tests were used as they were. This might be resulted from the difference of the stress gradient in the beam-columns and the stub columns. Consequently, the parameters other than the yield stress(σ_y), the tensile strength(σ_u), and the length of the inelastic joint are adjusted by trial and errors so that the monotonic curves simulated under constant axial loads totally match with the corresponding test curves. The length of the inelastic joint is assumed herein to be one-eighth of the column length. A set of model parameters arranged in such a manner is numerated in Table 4.

The monotonic curves predicted by the set of model parameters are shown in Figs. 6(b) and 7(b). The difference between the maximum resistance in the 'tension-side' loading case and that in the corresponding constant axial load case can not be simulated in the analysis, as shown in Figs. 7(a) and 7(b). The reason is that only a single set of model parameters are adopted in the analysis. As described before, the maximum resistance in these two cases are limited by the local buckling failure, and it is obvious that a single model of compression side skeleton curve could never explain such a difference in the local buckling strength. However, other aspects of the inelastic behaviors, such as the manner of the resistance deterioration and the maximum resistance controlled by the P-Δ effect, are well simulated by the present model with a single set of model parameters.

The two parameters associated with the hysteresis model, Ψ and r, are assumed to be 0.8 and 5, respectively, and the analyses are performed for the cyclic loading cases. The results are shown in Figs. 9(b) and 10(b). Basic aspects of hysteresis behaviors, such as the shape of the hysteresis loops and the maximum resistances in the both side loadings, are well simulated by the present model. Especially in the case of the varying axial load, the simulated hysteresis loops at each stage to the complete collapse fairly well agree with the test results.

5. CONCLUDING REMARKS

(1) H-shaped steel members are tested under uni-directional bending and a large amount of axial load change as well. Each specimen is assumed to be a side column at the lowest story of a tower-like high-rise building. Computer-controlled loading tests are performed, where the sub-structuring techniques are used to determine the varying axial load to be applied to the specimens. It is found that the deterioration of the lateral resistance resulted from such an intelligent testing is considerably different from the result of the ordinary testing under constant axial loads.

(2) A simplified constitutive modeling is also proposed for inelastic portions of steel beam-columns. The monotonic and the cyclic loading test results under varying axial load can be well simulated by the model with a single set of parameters so far as the parameters are calibrated to match with the monotonic curve under the constant axial load.

ACKNOWLEDGEMENTS

The authors would like to express their appreciation to Mr. Yosuke Shimawaki, Technical Official of Institute of Industrial Science, Mr. Carlos Alberto Zavala, Research student of Graduate School, University of Tokyo, for their supports during this study. Also, the authors would like to thank Professor Masayoshi Nakashima of Kobe University for his technical suggestions, and his graduate students, Mr. Maeda and Mr. Takaoka, for their participation and assistance during the experimental works.

REFERENCES

[1] K. Takanashi, H. Taniguchi, H. Tanaka: "Cyclic Loading Tests and a Numerical Analysis on H-shaped Columns under Bi-directional Horizontal Forces (Part 1 Inelastic response of H-shaped columns to Bi-directional horizontal earthquake ground motions)," Trans. of AIJ, No. 323, pp. 59-70, January 1983.

[2] C. Matsui, S. Morino, K. Tsuda: "An Experimental Study on Inelastic Behavior of Wide-Flange Steel Beam-Columns Under Constant Vertical and Two-Dimensional Horizontal Loads," Trans. of AIJ, No. 361, pp. 113-122, March 1986.

[3] Kang-ning Li et al.: "Behavior of Reinforced Concrete Columns under Varying Axial and Earthquake Loads (Part 1 Experiment)," Technical Papers of Annual Meeting of AIJ, pp. 379-382, Hokkaido, August 1986.

[4] E. Fukuzawa, Y. Isozaki, M. Takahashi:"Elastic-Plastic Analysis of Reinforced Concrete Frame in Consideration of Fluctuation of Axial Forces on Columns," Trans. of AIJ, No. 372, pp.31-44, February 1987.

[5] Y. Tatsumi, S. Otani, H. Aoyama:"Behavior of Reinforced Concrete Columns under Bi-directional Lateral and Large Varying Axial Loads," Journal of Structural Engineering, Vol. 36B, March 1990.

[6] K. Ohi, K. Takanashi, Ling-hua Meng: "Multi-spring Model for Inelastic Behavior of Steel Members with Local Buckling," Bull. of ERS, No. 23, March 1991.

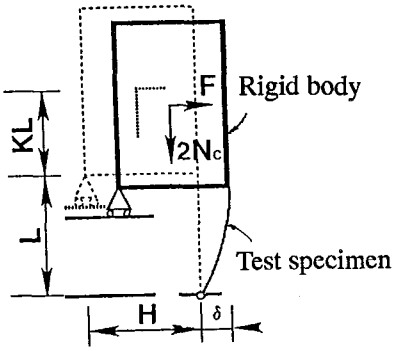

Fig.1 Fictitious Structural System Assumed in Intelligent Loading

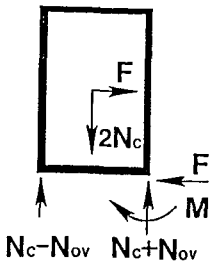

Fig.2 Forces Acting on the Rigid Body

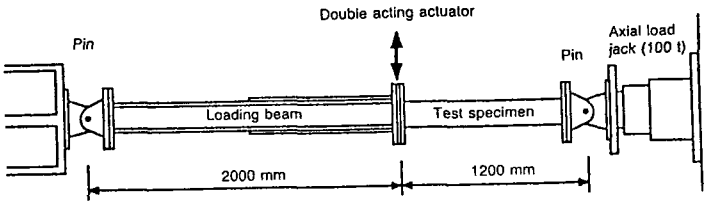

Fig.3 Test Setup

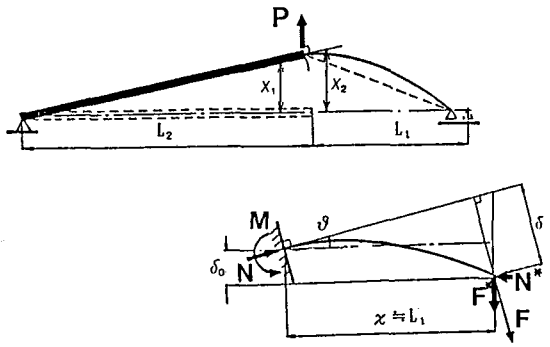

Fig.4 Loads and Displacements of Beam-Column Specimen

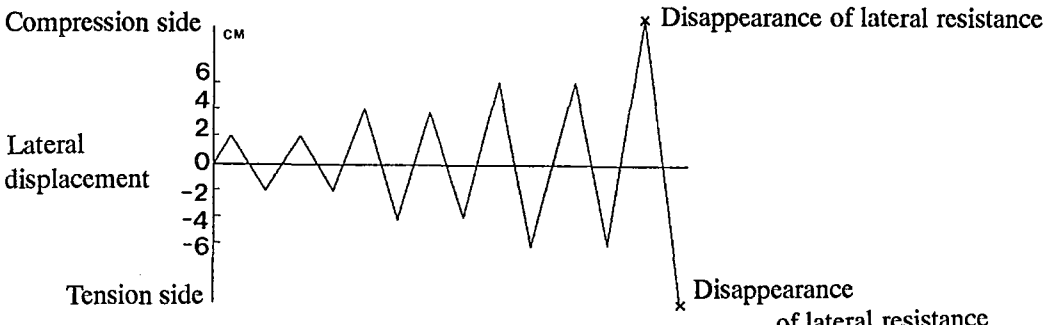

Fig.5 Displacement Control in Cyclic Loading Tests

Table 1 Dimensions of Specimens and Loading Types

Loading Type	B (cm)	H (cm)	t_f (cm)	t_w (cm)	A (cm^2)	I (cm^4)	Axial load (ton)
Mono	15.046	15.295	1.048	0.644	40.037	1726.6	53.6–73.2 (compression side)
Mono	15.018	15.226	1.038	0.567	38.633	1679.2	73.2 (constant)
Cyclic	15.053	15.258	1.022	0.617	38.921	1680.2	7.0–81.1 (varying)
Mono	15.044	15.301	1.018	0.640	39.119	1689.3	53.6–17.2 (tension side)
Mono	15.071	15.307	1.023	0.653	39.495	1702.4	17.2 (constant)
Cyclic	15.040	15.265	1.011	0.635	38.820	1670.2	53.6 (constant)

B: Width, H: Depth, t_f: Flange thickness, t_w; Web thickness,
A: Cross-sectional Area, I: Moment of inertia

Table 2 Mechanical Properties derived from Tension Tests

Test pieces	A (cm^2)	P_y (ton)	P_u (ton)	σ_y (t/cm^2)	σ_u (t/cm^2)	E_{st}/E	σ_y/σ_u (%)	δ_B (cm)	δ_B/L (%)
Flange	3.813	12.32	19.10	3.23	5.01	1/60	64.4	4.90	24.5
Flange	3.871	12.46	19.16	3.22	4.95	1/56	65.1	4.90	24.5
Flange	3.928	12.57	19.64	3.20	5.00	1/60	64.0	4.70	23.5
Flange	3.880	12.45	19.36	3.21	4.99	1/60	64.3	4.90	24.5
Web	2.635	9.01	13.28	3.42	5.04	1/60	67.9	5.30	26.5
Web	2.669	9.20	13.61	3.35	5.10	1/60	67.6	5.00	25.0

σ_y: Yield stress, σ_u: Maximum stress in tension, E: Elastic modulus,
E_{st}: Initial strain-hardening modulus, δ_B: Elongation at breaking

Table 3 Results of Stub Column Tests

B (cm)	H (cm)	t_f (cm)	t_w (cm)	A (cm^2)	L (cm)	N_y (ton)	N_m (ton)	σ_y (t/cm^2)	σ_m (t/cm^2)
15.038	15.237	0.968	0.650	38.76	45.00	133.30	150.00	3.44	3.87
15.073	15.256	0.983	0.680	39.67	45.01	138.80	160.60	3.50	4.05

σ_m: Maximum stress in compression

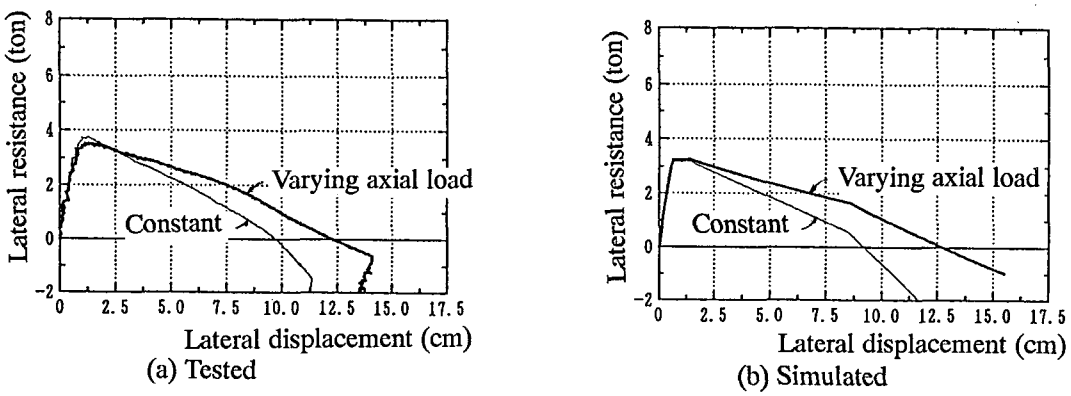

Fig.6 Lateral Resistance vs. Lateral Displacement
(Compression Side; Monotonic Loading Tests)

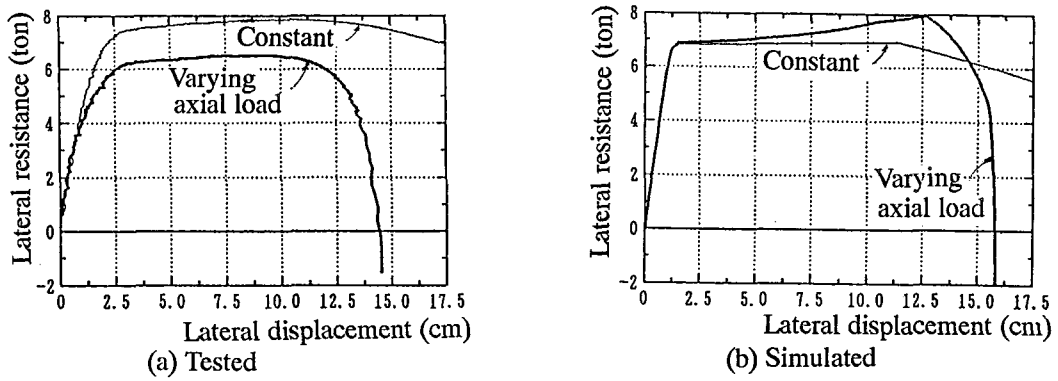

Fig.7 Lateral Resistance vs. Lateral Displacement
(Tension Side; Monotonic Loading Tests)

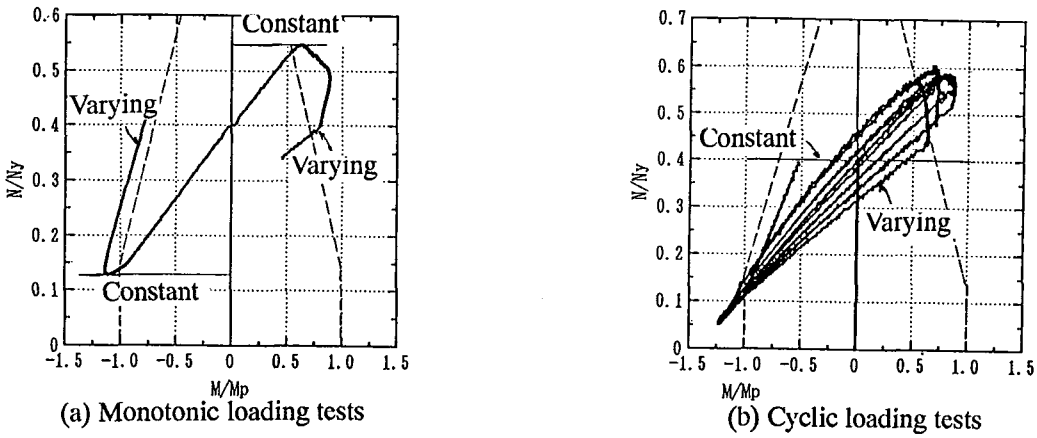

Fig.8 Axial Load vs. Bending Moment
(N_y: Yield axial load, M_p: Fully-plastic moment under no axial load)

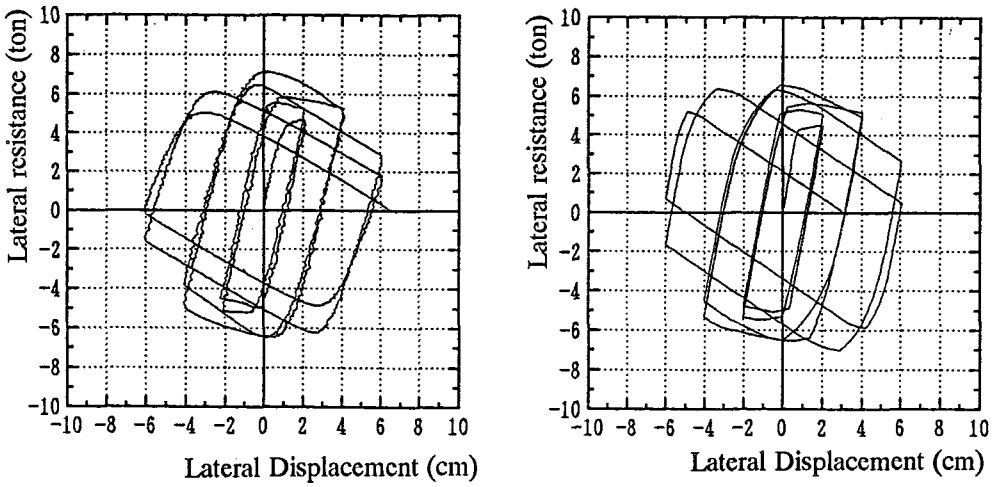

(a) Tested (b) Simulated

Fig.9 Hysteresis Loops Under Constant Axial Load

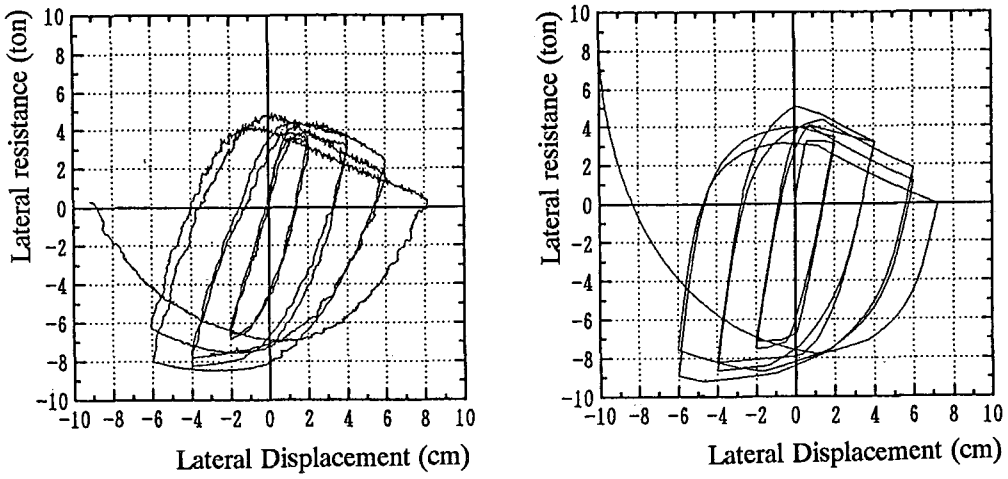

(a) Tested (b) Simulated

Fig.10 Hysteresis Loops Under Varying Axial Load

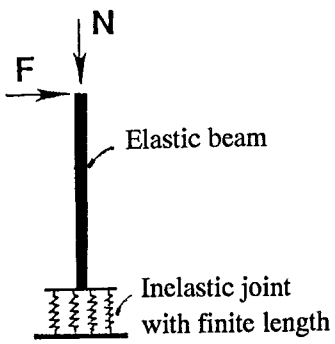

Fig.11 Simplified Beam-Column Model

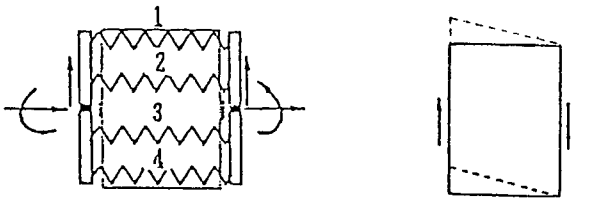

(a) Axial spring elements (b) Shear panel element

Fig.12 Elements of Inelastic Joint

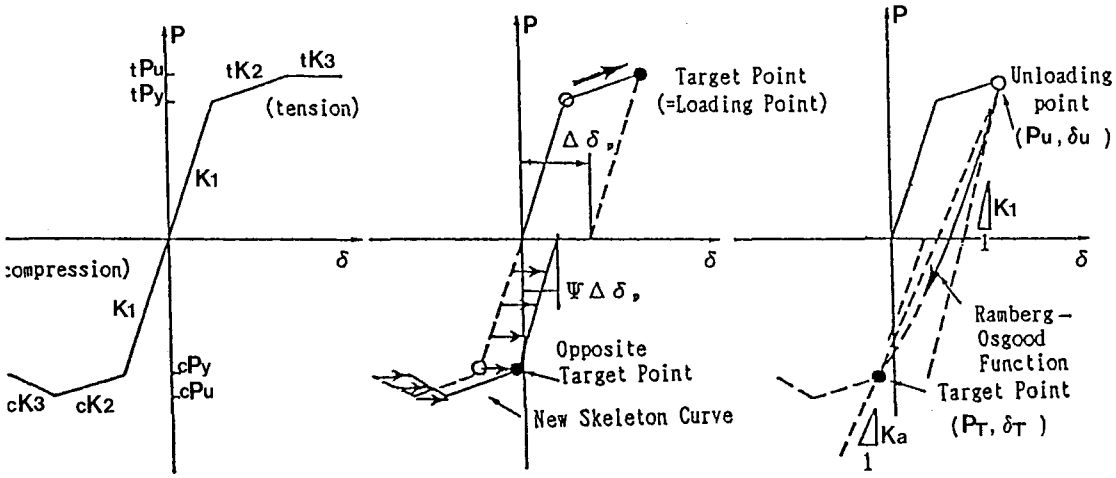

(a) Initial skeleton curve (b) Shift of skeleton curve (c) Unloading and reloading

Fig.13 Hysteresis Rule for Axial Spring Elements

Table 4 Model Parameters for Skelcton Curves

Spring No.	σ_y	σ_m	σ_u	K_1	$_cK_2$	$_cK_3$	$_tK_2$	$_tK_3$
1、4	3.3	4.2	5.0	540.8	3.60	-2.70	3.60	0.00
2、3	3.3	4.2	5.0	652.1	4.35	-3.26	4.35	0.00

Note: The length of the inelastic joint is kept 15 cm.